Novel Approach for Health Monitoring of Earthen Embankments

S. Utili[1]; R. Castellanza[2]; A. Galli[3]; and P. Sentenac[4]

Introduction

Earthen flood-defense embankments, also known as levees, are long structures usually made of local material available at the construction site. In the United Kingdom, flood-defense embankments are mainly made of cohesive soils, either clay or silt. Most of them were built before the development of modern soil mechanics in the eighteenth century (Charles 2008). Owing to their progressive aging, proper infrastructure condition assessment, based on sound engineering, is becoming increasingly important (Perry et al. 2001).

The formation of desiccation cracks in earthen embankments and tailing dams made of cohesive soils during dry seasons is detrimental to their stability (Rodriguez et al. 2007). Desiccation is responsible for the onset of primary cracks, which first appear at the surface, and then propagate downward, and for so-called secondary and tertiary cracks (Konrad and Ayad 1997). Desiccation-induced failures are deemed to become increasingly important as progressively more extreme weather conditions are predicted by climatologists to take place worldwide (Milly et al. 2002). Allsop et al. (2007) provide a comprehensive list of the several failure modes that may take place in earthen embankments. Several potential failure mechanisms are negatively affected by the presence of desiccation cracks, such as deep rotational slides starting from the horizontal upper surface (Utili 2013), shallow slides developing along the flanks (Aubeny and Lytton 2004; Zhang et al. 2005), erosion of the flanks by overtopping water [ASCE/EWRI Task Committee on Dam/Levee Breaching 2011] and/or wave action (D'Elisio 2007), and internal erosion (Wan and Fell 2004). In particular, the presence of cracks can substantially decrease the resistance of embankments with regard to overtopping and internal erosion, which alone count for 34 and 28%, respectively, of the embankment failures in the world (ASCE/EWRI Task Committee on Dam/Levee Breaching 2011).

Monitoring and condition assessment of flood-defense embankments worldwide are mainly carried out by visual inspections at set intervals (Morris et al. 2007; Andersen et al. 1999). In a few countries [e.g., the United Kingdom (Environment Agency 2006), Netherlands, and the United States], guidelines exist to rate the health/deterioration of embankments on the basis of a prescribed set of visual features. Unfortunately, this type of assessment is purely qualitative and relies heavily on the level of training and experience of the inspection engineer. So, there is consensus among experts on the fact that, although visual inspection provides valuable information, a meaningful and robust assessment of the fitness for the purpose of earthen flood-defense embankments cannot rely entirely on visual inspection (Allsop et al. 2007). On the other hand, intrusive tests (e.g., the cone penetration test, piezocones, vane tests, or inclinometers) are impractical for the monitoring of long structures like embankments, given the necessity of performing tests in several locations to account for the typical high variability of the ground properties. The same applies to standard geotechnical laboratory tests, which involve time-consuming retrieval and transportation of samples to the laboratory.

In this paper, a cost-effective approach using a suite of geotechnical and geophysical probes is proposed for the long-term monitoring of the variation of water content in the ground and of the susceptibility to desiccation-induced fissuring. The methodology is simple and modular (i.e., the level of sophistication/accuracy is a function of the financial resources available), and it can be

[1]Associate Professor, School of Engineering, Univ. of Warwick, Coventry CV4 7AL, U.K.; formerly, Lecturer, Univ. of Oxford, Oxford OX1 3PJ, U.K.; formerly, Postdoctoral Research Fellow, Dept. of Civil Engineering, Univ. of Strathclyde, Glasgow G1 1XQ, U.K. (corresponding author). E-mail: S.utili@warwick.ac.uk

[2]Associate Professor, Dept. of Earth and Environmental Sciences, Univ. degli Studi di Milano-Bicocca, Milano 20126, Italy.

[3]Assistant Professor, Dept. of Civil and Environmental Engineering, Politecnico di Milano, Milano 20133, Italy.

[4]Lecturer, Dept. of Civil Engineering, Univ. of Strathclyde, Glasgow G1 1XQ, U.K.

Note. This manuscript was submitted on December 30, 2013; approved on September 9, 2014; published online on November 7, 2014. Discussion period open until April 7, 2015

readily implemented by the authorities in charge of the management of earthen flood-defense embankments and tailing dams.

Conceptual Framework

The methodology proposed here is based on the assumption that water content can be selected as a direct indicator of the occurrence of extensive fissuring in the ground, as suggested by Dyer et al. (2009) and Tang et al. (2011). The authors are aware that a lot of research has been performed recently to successfully relate the onset of cracks to soil suction (e.g., Shin and Santamarina 2011; Muñoz-Castelblanco et al. 2012b). However, as recently well illustrated by Costa et al. (2013), the formation and propagation of cracks in cohesive soils also depend on several other factors, such as the drying rate and the amount of fracture energy involved in crack propagation. Considering flood-defense embankments, the loss of structural integrity (i.e., the loss of the structure's capacity to withstand the design hydraulic load) occurs when desiccation fissuring progresses to the extent that an interconnected network of cracks is formed rather than when surficial cracks first appear. Therefore, the approximation introduced in relating the loss of structural integrity to a threshold value of suction appears no less important than the approximation introduced in relating the loss of structural integrity to a threshold value in terms of water content. Moreover, the cost of monitoring suction in a long embankment for an extended period of time is very significant, with the extra burden of necessitating complex installation and maintenance procedures for the probes needed to measure suction. These reasons underpin the authors' choice of monitoring the groundwater content.

The position of any point in a long linear structure like an embankment or tailing dam can be defined according to either a global Cartesian coordinate system (X, Y, Z) or a local coordinate system defined at the level of the structure's cross sections. For the sake of simplicity, the following choice was made: a curvilinear global coordinate, s, running along the longitudinal direction of the structure, which uniquely identifies the location of any cross section; a local Cartesian coordinate, x, lying in the horizontal plane and perpendicular to the s-coordinate; and a vertical downward Cartesian coordinate, z, which can be thought of as both a global and local coordinate. So, the water content, w, at a generic point of the earthen structure is a function of these three spatial coordinates and of time: $w(x, s, z, t)$. A local tangential coordinate s_t was also defined, as shown in Fig. 1(b). The procedure proposed to determine the function $w = w(x, s, z, t)$ in the whole embankment is based on the following actions:

1. Measurement of the water content profile along a vertical line P of coordinates x_P, s_P at any time and depth $w(x = x_P, s = s_P, z, t) = w_P(z, t)$;
2. Measurements in some selected cross sections, located at $s = s_i$ (herein the subscript i is an integer identifying the embankment cross section considered), at some discrete time points t_k

(a)

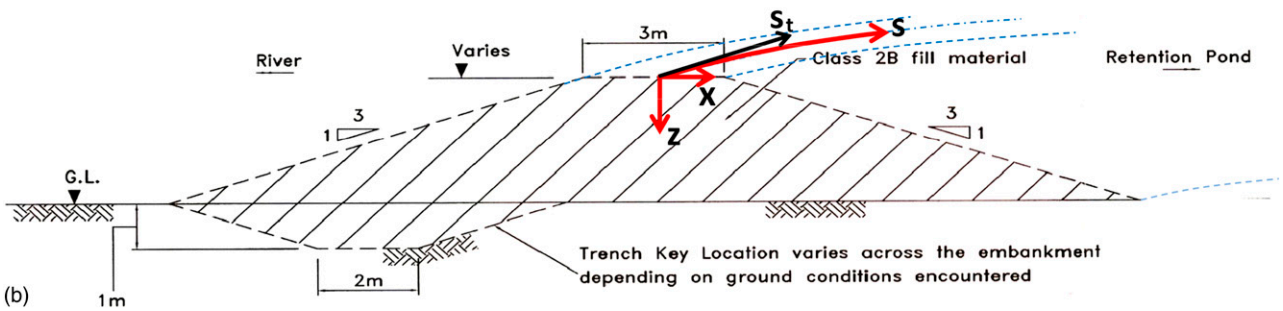

(b)

Fig. 1. (a) Plan view of monitored embankment (© Google, Image ©2014 Getmapping plc); (b) typical embankment cross section and system of coordinates adopted in paper

(herein the subscript k is an integer identifying the time point considered) of the function $w(x, s = s_i, z, t = t_k) = w_{i;k}(x, z)$;
3. Measurement by geophysical techniques of the water content at predefined time points, t_k, along the entire embankment (i.e., for any value of s); and
4. Evaluation by extrapolation of the water content at any point at any time: $w(x, s, z, t)$.

Once the water content function $w(x, s, z, t)$ is determined, an index quantifying the susceptibility of any cross section of the embankment to desiccation fissuring can be defined and a map of susceptibility can be generated to identify the most critical zones of the structure; see the "Proposal for Susceptibility Index to Desiccation Fissuring" section. The map is useful to set priorities for intervention in the zones requiring remedial actions.

Description of Site

In 2007, the construction of an earthen flood-defense embankment enclosing a floodplain along the river Irvine to drain excess waters from the river during floods was completed in Galston (Scotland, United Kingdom). The embankment is made of an uppermost layer (5–10 cm) of a sandy topsoil, below which lies a core of glacial till containing several boulders (Fig. 1). Grass roots do not extend beyond the topsoil. A typical cross section is sketched in Fig. 1(b). Although the inclination of the flanks is rather uniform, the sizes of the flanks and of the upper surfaces vary quite substantially along the longitudinal direction, giving rise to a nonnegligible spatial variation of the geometry of the cross sections, which may have consequences in terms of the spatial variation of the water content in the ground; see the "Monitored Data" and "Extrapolation of Water Content Function for Entire Structure" sections.

A number of standard geotechnical tests were carried out to characterize the ground properties: measurements of the gravimetric moisture content, void ratio, particle size distribution, and Atterberg limits were taken. The grain size distribution of both the topsoil and the glacial till was determined according to ASTM E11 (ASTM 2013) (Fig. 2).

Monitoring System

In the following, the main geotechnical and geophysical measurements of the monitoring system are described. The main technical features of all the probes used in the monitoring program (e.g., the manufacturer, accuracy, and operational range) are given in Table 1.

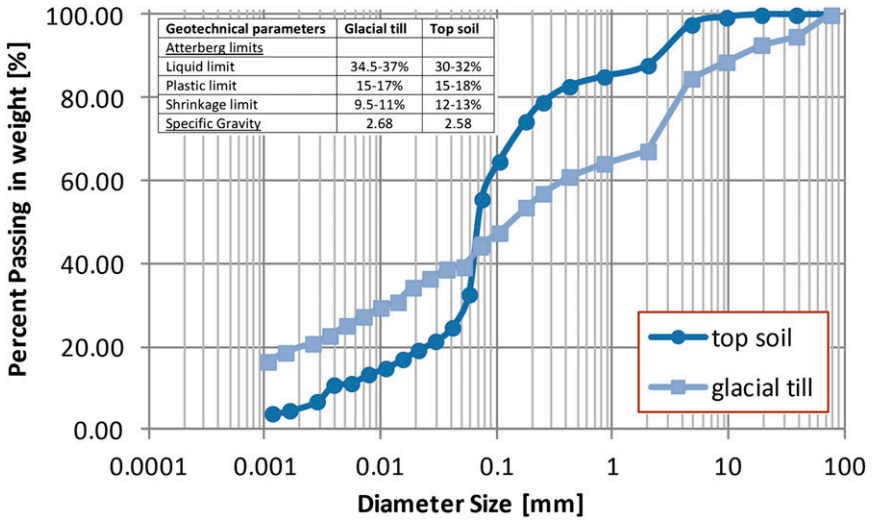

Fig. 2. Particle size distribution of glacial till and of topsoil and main geotechnical indexes

Table 1. Main Technical Features of Probes Used for Monitoring

Device	Product name	Manufacturer	Accuracy and operational range
Equitensiometer	EQ2	Delta-T Devices (http://www.delta-t.co.uk/)	±10 kPa from 0 to −100 kPa; ±5% from −100 to −1,000 kPa
Theta probe	THP	Delta-T Devices (http://www.delta-t.co.uk/)	After calibration to a specific soil type ±0.01 $m^3 \cdot m^{-3}$ from 0 to 0.4 $m^3 \cdot m^{-3}$ with temperature from −20 to 40°C
Profile probe	PR2	Delta-T Devices (http://www.delta-t.co.uk/)	After calibration to a specific soil type ±0.04 $m^3 \cdot m^{-3}$ from 0 to 0.4 $m^3 \cdot m^{-3}$; reduced accuracy from 0.4 to 1 $m^3 \cdot m^{-3}$
Diviner	Diviner 2000	Sentek (http://www.sentek.com.au)	±0.003% volume from −20 to 75°C
Weather station	iMETOS pro	Pessl Instruments (http://metos.at/joomla/page/)	Temperature ±0.1°C from −40 to 60°; relative humidity 1% from 0 to 100%; wind speed 0.3 m/s from 0 to 60 m/s; precipitation ±0.1 mm
Electromagnetic probe	CMD-2	GF Instruments (http://www.gfinstruments.cz)	±4% at 50 mS/m; operating temperature −10 to 50°C; maximum sampling rate 10 Hz

Measurement of Water Content along Selected Vertical P

In Fig. 3(b), the vertical line *P* is plotted with the label PR2_E2. A data logger reading data at an hourly frequency was installed into a bespoke metallic fence close to the vertical line *P* [Fig. 3(c)]. As schematically shown in Figs. 3(a and b), the following devices were connected to the data logger:

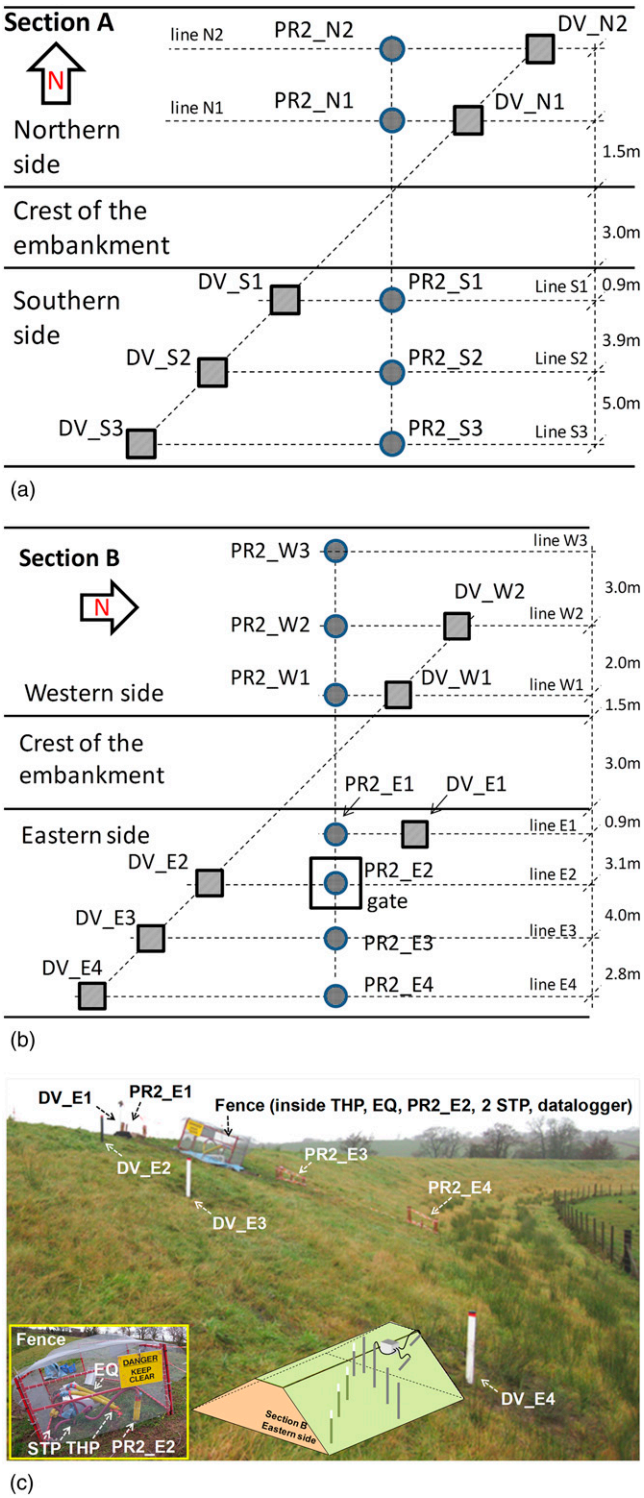

Fig. 3. Position of access tubes for profile probe (PR2) and diviner (DV): (a) plan view of Section A; (b) plan view of Section B; (c) view of cross Section B from eastern side

- A theta probe (THP) (THP, Delta-T Devices, Cambridge, United Kingdom) made of four metal rods to be inserted in the ground to measure its water content at a depth of 25 cm: special care was taken to avoid the formation of any air gaps between the prongs of the probe and the surrounding soil by prefilling the augered holes hosting the probes with a slurry and pushing the probe into undisturbed soil well beyond the hole bottom; the device takes a measurement of the relative permittivity (also commonly called the dielectric constant) of the ground, which is then converted into gravimetric water content;
- An equitensiometer (EQ) (EQ2, Delta-T) to measure suction up to a maximum value of 1,000 kPa at the same depth of 25 cm: this device consists of THP pins embedded into a porous matric;
- A portable profile probe (PR) (PR2, Delta-T Devices), which is based on time-domain reflectometry, to measure the water content at six different depths from the ground surface (10, 20, 30, 40, 60, and 100 cm); and
- Two temperature probes inserted at 25 and 40 cm of depth in the ground.

Measurement of Water Content at Cross Sections A and B

To evaluate the water content in the ground up to 1 m of depth, several access tubes were drilled into two cross sections [A and B in Figs. 3(a and b)] that were perpendicular to each other to better account for the influence of topographical orientation on the measured water content; see the "Extrapolation of Water Content Function for Entire Structure" section. Special care was taken to avoid the formation of any air gaps between the tubes where the PR was inserted and the surrounding soil. Two different instruments were used:

- The PR, already described in the previous section, to measure the groundwater content along several vertical lines up to a depth of 1 m; and
- A portable diviner (DV) [Diviner 2000, Sentek, Stepney, Australia (Table 1)] to measure the groundwater content along various vertical lines every 10 cm from ground level down to 1.6 m of depth. This device is based on frequency-domain reflectometry.

In Section A, 10 access tubes were used: five were used for the PR (labeled PR2_xx), and five were used for the DV (labeled DV_xx). In Section B, there were 12 measuring points: six were used for the PR, and six were used for the DV. Some of the access tubes for the PR and the DV were laid down so as to be aligned along the longitudinal direction of the embankment to perform a cross comparison between them, as will be shown in the "Calibration of Geotechnical Suite" section [Figs. 3(a and b)]. A weather station [iMETOS pro, Pessl Instruments, Weiz, Austria (Table 1)] was installed 200 m south of Section B of the embankment to collect data on rainfall precipitation, air humidity, temperature, and wind speed over the 2-year period of monitoring.

Geophysical Measurements

Electromagnetic surveys present the advantages of being nonintrusive and quick to be carried out. Electromagnetic probes can measure the electrical conductivity of the ground. The CMD-2 probe [GF Instruments, Brno, Czech Republic (Table 1)] was chosen because it was a relatively cheap device that was simple to use (i.e., it did not require specific training). The working principles of the device are shown in GF Instruments (2011). Measurements were taken by an operator walking on the horizontal upper surface of the embankment along the longitudinal direction at a constant pace of 5 km/h, holding the CMD-2 approximately 1 m above ground, and orienting the device

perpendicular to the longitudinal direction so that the electromagnetic flow lines always lie in the plane perpendicular to the longitudinal direction (i.e., the plane of the embankment cross section).

Electrical resistivity tomography (ERT) is also a well-established geophysical technique that is increasingly used to measure electrical conductivity at the ground surface (Muñoz-Castelblanco et al. 2012a). Nowadays, three-dimensional (3D) maps of in situ water content can be generated from ground-resistivity measurements, as shown in De Vita et al. (2012) and Di Maio and Piegari (2011), once appropriate correlations between ground resistivity and in situ water content have been established. The potential for obtaining 3D maps of water content makes ERT look like a very attractive tool for the monitoring of embankments. However, ERT appears to be impractical for the continuous monitoring of an extended structure over long time spans, because it requires operators possessing the specialist skills to install the electrodes of the devices in the ground and operate them. For this reason, to take geophysical measurements of electrical conductivity in the embankment ("Integration of Geophysical Data with Geotechnical Suite" section), the authors chose to use electromagnetic probes instead. Nevertheless, in the authors' opinion, ERT could still be beneficially used in the zones of the embankment identified as critical by the integrated geotechnical/geophysical approach proposed here. In fact, ERT is useful for investigating in great detail the state of fissuring of the ground in zones of limited extent.

Calibration of Geotechnical Suite

A key point of any monitoring system is the proper calibration of all the used devices. Regarding the calibration exercise undertaken, only the glacial till is of interest, because the thickness of the topsoil in the embankment flanks, where all the measurements were taken, is 5 cm, and the measurements were taken at depths that were always larger than 10 cm. A sequential approach was adopted, which is detailed in the following.

Direct Calibration of THP

The calibration curve for the THP was taken from Zielinski (2009) (Fig. 4), who calibrated the THP using samples of till retrieved from the same quarry (Hallyards Quarry, Scotland, United Kingdom) from which the till of the monitored embankment was extracted. The till was retrieved from the quarry at five different known water contents and compacted into five cylindrical containers with the same compaction effort as in the monitored embankment [i.e., relative compaction of 95% with compaction control performed according to the *Specification for Highway Works: Earthworks, Series 0600* (Highways Agency 2006)]. Given the high level of compaction and the nonswelling nature of this glacial till, the variations of dry unit weight in the embankment over time and space occurring for the range of the measured in situ water contents can be considered negligible (less than $\pm 5\%$). Hence, the authors transformed the volumetric water contents measured by the geotechnical probes (PR, DV, etc.) into gravimetric water contents assuming the dry unit weight of the till at its optimal water content (i.e., a maximum dry unit weight of 19.1 kN/m^3). This value was obtained as the average of seven measurements performed in the laboratory on undisturbed U-38 samples retrieved from the embankment. This value turned out to be almost identical to the value measured by Zielinski et al. (2011) on a small-scale embankment built from the same glacial till reconstituted in the laboratory.

Indirect Calibration of PR

The calibration of the PR was obtained by comparing the raw data in millivolts obtained by the PR located at the gate in Section B (PR2_E2 in Fig. 3) at 20- and 30-cm depths with the measurements of the THP in the same location (20 cm longitudinally away from the PR2_E2 in Fig. 3) at a 25-cm depth for a 4-month period. Data were recorded every 4 h. A strong similarity between the trends of the readings of the two probes plotted in Fig. 5 was observed. Because the two devices measure the water content of the same portion of soil, a calibration procedure, based on the visual match of the curves, was adopted: the scale of the ordinate axis of the THP readings (expressed in millivolts) was varied until it satisfactorily matched the average (not reported in the figure to avoid cluttering) of the two measurements at 20- and 30-cm depths obtained by the THP. The resulting linear relationship between the values measured by the PR and the values measured by the THP is shown in Fig. 5. This relationship was used to convert the readings of the PR into equivalent millivolt units measured by the THP, and they were in turn transformed into gravimetric water content using the calibration curve of the THP (Fig. 4).

Indirect Calibration of DV

Following the same approach described in the previous section, indirect calibration of the DV was performed by varying the scale of the frequencies measured by the DV until a satisfactory match with the water content profile measured by the PR in the corresponding access tube was obtained. The corresponding PR access tube is the one aligned with the DV tube in the longitudinal direction [e.g., DV_S3 and PR2_S3 in Fig. 3(a)]. In Fig. 6(a), two of the performed calibrations are shown. The curve shown in Fig. 6(b) was obtained

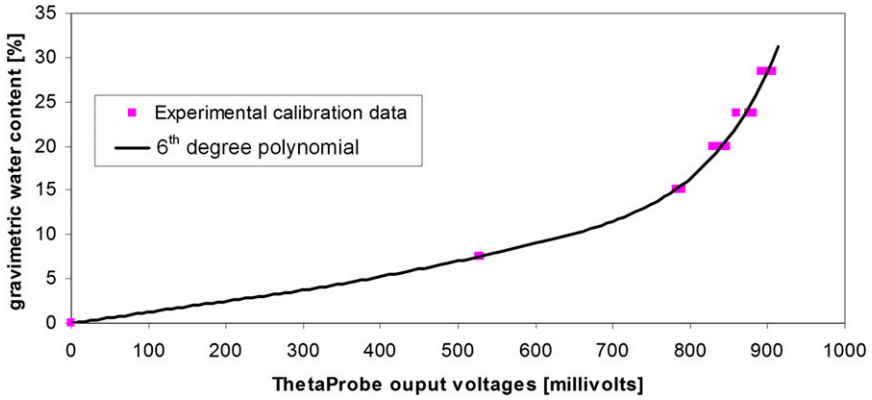

Fig. 4. Calibration curve for THP (experimental calibration data from Zielinski 2009)

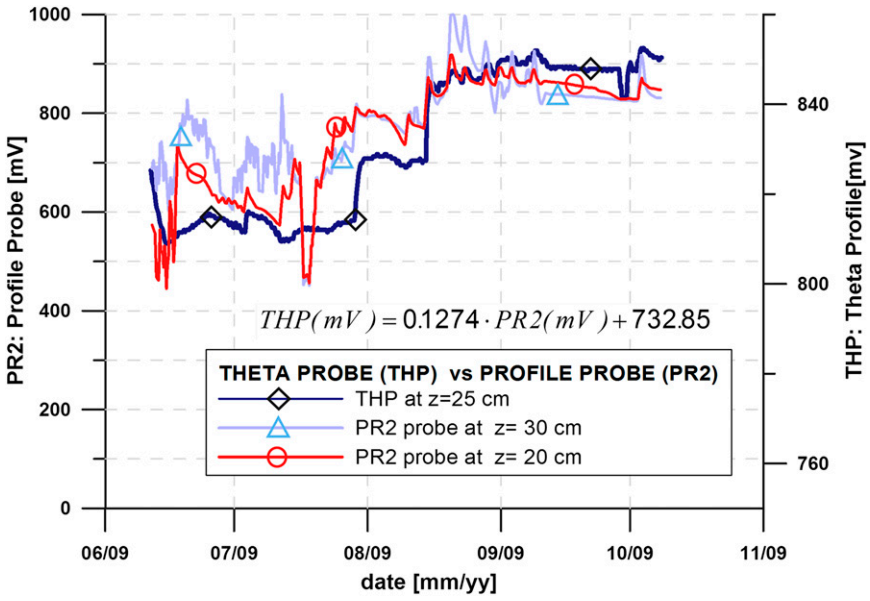

Fig. 5. Calibration of PR: measurements by THP and PR taken at same location, PR2_E2 (Fig. 3)

by repeating this procedure for all the monitoring points of the DV in the time period considered.

Because the calibration procedures adopted for the PR and the DV are based on cross correlation, errors of measurement could be amplified. Hence, to check the amount of error amplification, direct measurements of the gravimetric water content were obtained via small in situ samples taken at several points of the embankment on the same day; see the triangles in Fig. 6(a). Looking at Fig. 6(a), a good agreement between the values of water content measured by the indirectly calibrated probes (PR and DV) and direct measurements emerges, so it can be concluded that error propagation is within acceptable limits.

Overall, the adopted calibration procedure has the obvious advantage of requiring only small samples of soil for the direct calibration of the THP in the laboratory with the PR and DV indirectly calibrated in situ. Conversely, direct calibration of the PR and DV would require retrieving large volumes of soil, to avoid the influence of boundary effects, at predefined water contents to the laboratory.

Monitored Data

In this section, data relative to rainfalls, wind speed, relative humidity, air, and ground temperature recorded by the weather station installed near the embankment are analyzed and compared with the groundwater content recorded by the geotechnical suite in Cross Sections A and B. The purpose of this analysis was first to establish the variation in time and space of the water content and second to identify correlations between weather variables and groundwater content to separate out the variables significantly affecting the water content from the ones with a marginal influence, which therefore can be discarded from the monitoring program.

In principle, it would be possible to calculate the effective amount of rainfall infiltrating the ground from the calculation of evapotranspiration rates and the measurement or calculation of the amount of water runoff (Smethurst et al. 2012; Xu and Singh 2001). However, the amount of runoff is likely to depend strongly on the inclination of the embankment flanks, which varies locally, and to a lesser extent on to the local vegetation cover. Moreover, a reliable estimate for a long linear structure with varying cross-sectional geometries would require several points of measurement. This is against the overall philosophy of the proposed methodology, which aims to be as practical and simple as possible. Hence, the authors sought a relationship between in situ water content and total precipitated rainfall. The latter can be measured directly by a nearby weather station. Furthermore, in the United Kingdom at least, weather stations can be found in several localities, so often there will be no need to install a new station at the site of interest. In summary, on one hand using total rainfall makes the correlation with the in situ water content weaker because of the extra approximation of disregarding the variation of effective rainfall in the ground due to local lithological and geometrical variations; on the other hand, it is far more desirable for the authorities in charge of the monitoring system, because total rainfall is much easier to ascertain.

Continuous Measurements of Water Content Profiles

Data were recorded over a 2-year period. Here, only an extract of two significant periods is provided to show the seasonal trends of desiccation and wetting of the embankment. The most significant seasons are summer (Fig. 7) and winter. In Fig. 7(a), the groundwater content profile is plotted together with the recorded daily rainfall precipitation. Precipitations larger than approximately 5 mm/day or reaching 5 mm over a period of consecutive daily rainfalls lead to noticeable increases of water content apparent in the spikes of the curves relative to the water contents measured at 10- and 20-cm depths. No significant variations of water content were ever recorded at depths larger than 60 cm.

In the upper part of Fig. 7(a), the suction measured by the EQ2 at a 25-cm depth is plotted. It emerges that the suction is well related to the rainfall records as well as to the variation of the water content. The THP measured the water content at the same depth as the suction measurements of the EQ at a point 15 cm away along the horizontal direction so that an in situ suction-water characteristic curve (SWCC) for the considered point (PR2_E2) can be obtained (Curve C in Fig. 8). Zielinski et al. (2011) measured the SWCC of this glacial till in the laboratory with different techniques (Curve A in Fig. 8) and the SWCC (Curve B in Fig. 8) in a small-scale embankment made of the same material. In Fig. 8, all of these curves are plotted. Comparing the curves, it emerges that the values of in situ suction measured by the EQ lie close to the SWCC curves

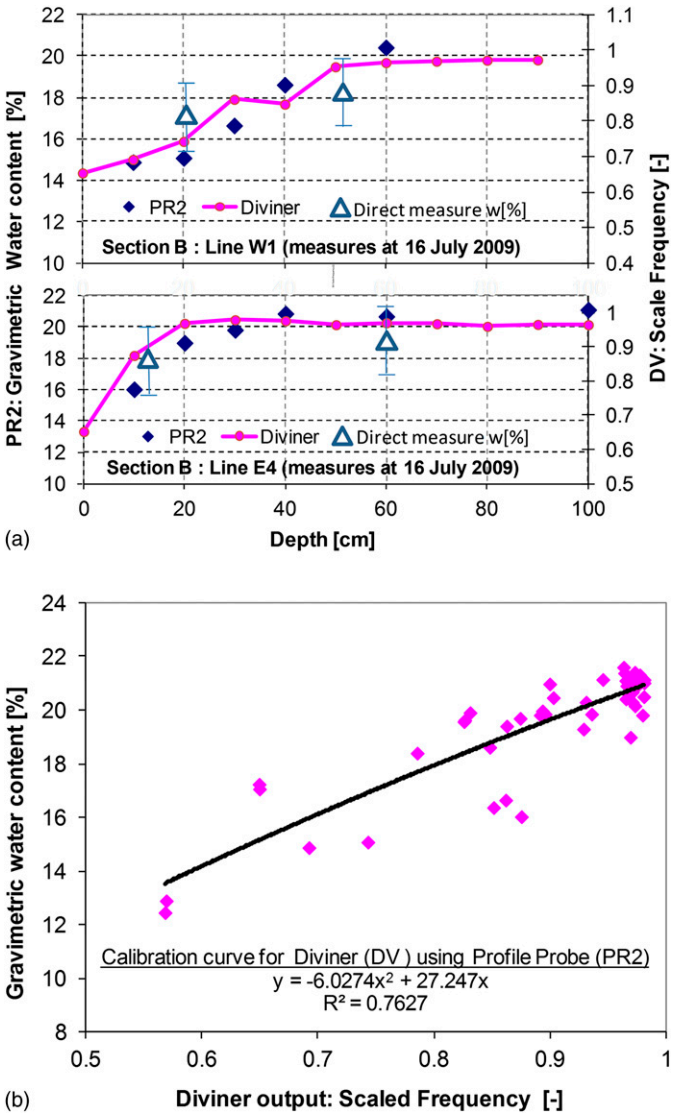

Fig. 6. Calibration of DV by comparison with measurements of PR: (a) examples of cross comparisons for measurements taken in access tubes lying along Longitudinal Lines W1 and E4 (Fig. 3 shows location of lines); triangles with their error bar indicate values of water content obtained via direct measurement; (b) obtained calibration curve for DV

obtained in the laboratory, and the boundaries of the hysteresis cycles are close. This result is quite remarkable.

Examining the recorded temperatures of the air and ground, a clear correlation between the two is found: in Fig. 7(b), the average between the maximum and minimum daily air temperature turns out to be very close to the ground temperature at a 10-cm depth. Relative humidity and wind speed were rather constant during the monitored period [Fig. 7(c)].

In the winter (Fig. 9) higher precipitations take place, leading to significantly larger quick increases of the groundwater content, in particular at shallow depths (10 cm). Because suction remained negligible for the entire period, the variation of suction over time is omitted from Fig. 9(b). The same remarks as for the summer period can be made, with the exception of the wind speed, which varies significantly more than during the summer period.

From the monitored data, it can be concluded that the groundwater content is highly sensitive to the amount of total precipitation and to the length of the dry periods, whereas no significant correlation to the relative humidity or to the variation of wind speed was found. These observations lead to the statement that, in principle, it is possible to estimate the water content in a cross section, and in turn the cross-sectional susceptibility to desiccation fissuring ("Proposal for Susceptibility Index to Desiccation Fissuring" section), from knowledge of both the groundwater content at the initial time of monitoring and the historical rainfall records. Given the limited resources available in this project, continuous measurements in time are available only in one section of the embankment, which is too little to validate a reliable correlation between the historical rainfall records and the water content. However, in light of the results obtained here, the authors suggest that if a sufficient number of sections are instrumented, a reliable correlation may be established so that meteorological data (especially rainfall records) could be used to infer the amount of water content along the entire embankment at any time according to the methodology presented in the next section ("Extrapolation of Water Content Function for Entire Structure" section) and to monitor the susceptibility of the structure to desiccation fissuring, as expounded in the "Proposal for Susceptibility Index to Desiccation Fissuring" section. This methodology would have the advantage of not requiring periodic walk-over surveys; it would only require the presence of a weather station near the structure.

Time Discrete Measurements of Water Content Profiles

To evaluate $w_{i;k} = w(x, z) = w(x, s = s_i, z, t = t_k)$, measurements were taken from the PR and the DV up to a depth of 1 m (Fig. 10). In Figs. 11(a and b), the evolution of the water content over time is plotted for Sections A and B, respectively. These figures were obtained by interpolating in space the values of the water content measured from the locations of the monitoring points (Fig. 3). The analyzed domain consists of the uppermost 1 m of the cross sections, because no significant variations of water content were ever observed at larger depths (Figs. 7 and 9). To generate the plotted contours of water content, first a mesh was created whose nodes coincided with the locations of the readings taken from the PR and the DV, and then postprocessing FEM software, called *GiD* (International Center for Numerical Methods in Engineering 2014), was used to interpolate the values along the x- and z-coordinates. The interpolation was repeated for measurements taken at different times (Fig. 11). From these data, it emerges that the water content varies significantly between the two sections. The dependence of the water content on the geometrical alignment of the cross sections has been accounted for in deriving the function $w(x, s, z, t)$, as will be shown in the next section.

Extrapolation of Water Content Function for Entire Structure

In the following, first $w(x, s, z, t)$ will be derived on the basis of data gathered by the geotechnical suite only. Second, it will be derived using measurements of electrical conductivity taken by the CMD-2 probe.

Derivation of Water Content Function from Data Retrieved by Geotechnical Suite

In Fig. 11, the water content of the two monitored cross sections (A and B) is plotted. The water content in any other cross section is different owing to two main factors:

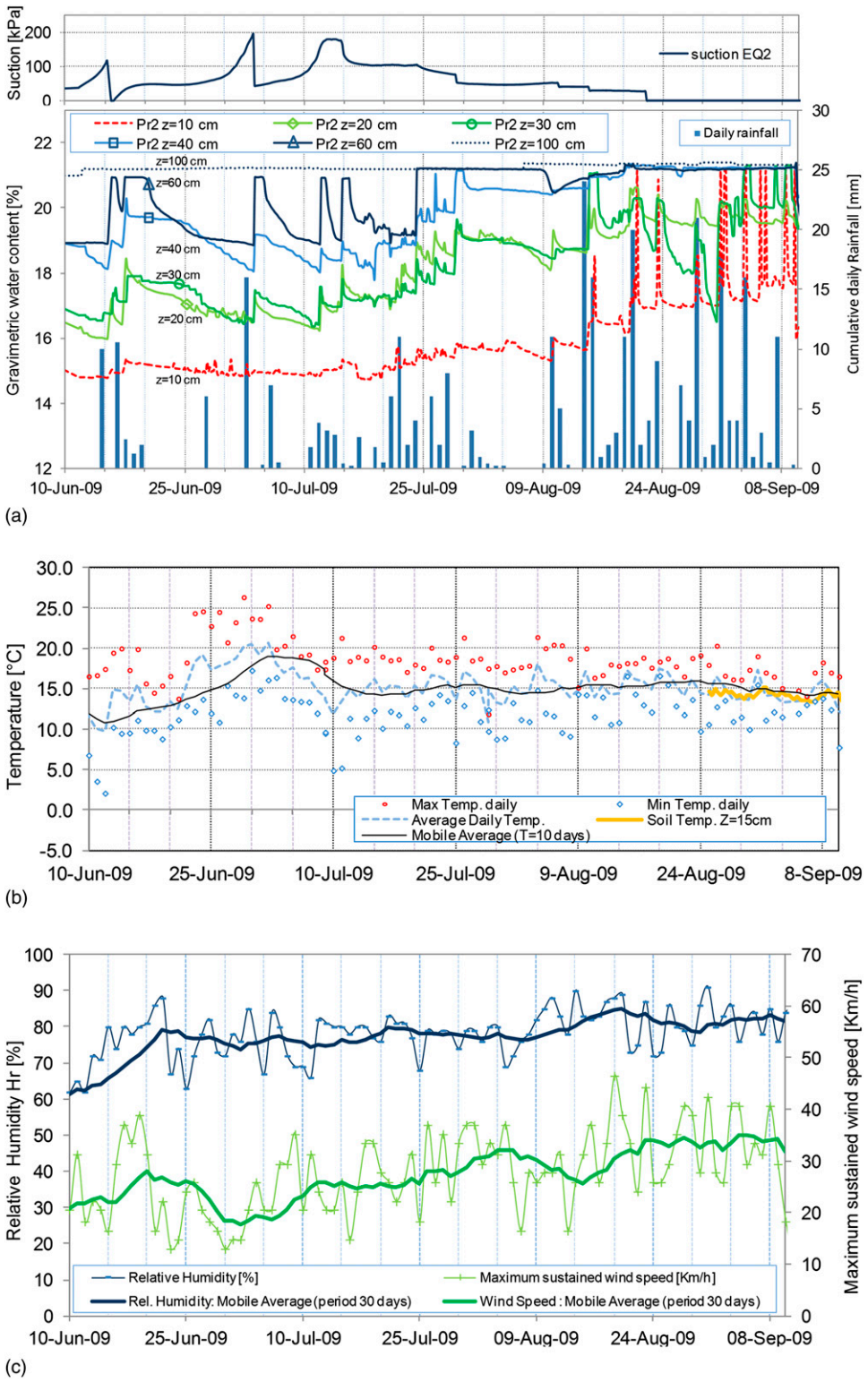

Fig. 7. Summer 2009 (Section B): (a) evolution of gravimetric water content, suction, and rainfall record; (b) average of maximum and minimum daily air temperature and ground temperature measured at 10-cm depth; (c) relative humidity and wind speed: thin line follows daily variation, whereas thick line is mobile average over 10 days

1. Different exposure to weather conditions (e.g., sunlight, rainfall, and wind), which is a function of the local orientation of the considered cross section with respect to north; this factor affects the groundwater content along the flanks of the embankment much more than that underneath the horizontal upper surface.
2. Spatial variation of the geometrical, hydraulic, and lithological properties of the cross sections along the longitudinal coordinate *s*: heterogeneities in the compaction processes during construction, for example, are likely to cause a non-negligible spatial variation of the hydraulic conductivity

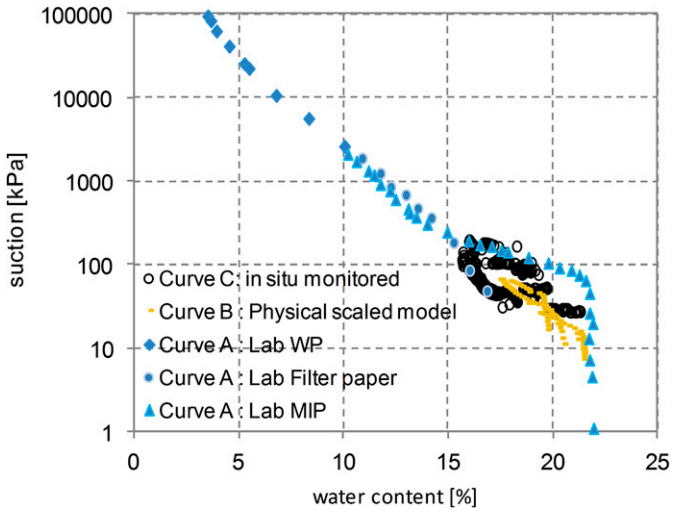

Fig. 8. Comparison of in situ SWCC derived from measurements taken by THP and EQ at 25-cm depth (Curve C) with SWCC determined from reconstituted samples (Curve A data from Zielinski et al. 2011) and in small-scale embankment model (Curve B data from Zielinski et al. 2011)

along the longitudinal direction. Concerning compositional or lithological variability, this is likely to be small for the embankment examined here owing to the facts that it is made of homogeneous material and is young. However, in general, old earthen embankments are very often highly heterogeneous, comprising a mixture of several materials locally available at the time of construction.

Regarding Factor 1, considering the axis of symmetry of the cross section [axis z in Fig. 1(b)], exposure to each single weather element (e.g., wind, sunrays, or rainfall droplets) gives rise to a variation of water content that is either antisymmetrical or nil in the case of equal exposure (e.g., no wind and vertical sunrays), but the combination of the single weather elements (e.g., the sum of the antisymmetrical variations of water content due to exposure to wind or exposure to sunrays) may give rise to a nonnegligible symmetrical variation of water content as well. The antisymmetrical part is a function of the orientation of the cross section considered, whereas the symmetrical one is a function of the longitudinal coordinate s. Regarding factor 2, geometrical, hydraulic, and lithological variations in the embankment imply a variation of water content, which in the authors' opinion is much larger along the longitudinal coordinate s than within each single cross section and therefore is mainly symmetrical. In summary, the water-content variation in the embankment depends on both cross-sectional orientation and cross-sectional position. The latter is expressed by the longitudinal distance from a reference cross section (coordinate s). To better account for the variation of water content due to these geometrical factors, cross-sectional orientation and cross-sectional position, it is convenient to split the water content function, $w(x, s, z, t)$, into two parts, a symmetrical part, w^s, and an antisymmetrical one, w^a, with respect to the axis of symmetry of the cross section

$$w^s(x,s,z,t) = \frac{w(x,s,z,t) + w(-x,s,z,t)}{2} \quad \text{and}$$
$$w^a(x,s,z,t) = \frac{w(x,s,z,t) - w(-x,s,z,t)}{2} \tag{1}$$

To account for the influence of cross-sectional orientation, it is convenient to use a function $\theta(s)$, with θ being the angle between s_t, the direction normal to the cross section, and a reference direction here chosen as the geographical north [Fig. 12(a)]. Considering the measurements of water content at discrete time points t_k, $w^a_k(x,s,z) = w^a(x,s,z,t=t_k)$ can be expressed as the weighted average of the values of water content, $w^a_{i;k}(x,z) = w^a(x,s=s_i,z,t=t_k)$, recorded at $t=t_k$ in the N instrumented cross sections

$$w^a_k(x,s,z) = w^a(x,s,z,t=t_k) = \sum_{i=1}^{N} w^a_{i;k}(x,z)\cdot\alpha_i(\theta) \tag{2}$$

with $\alpha_i(\theta)$ = weight functions accounting for the antisymmetrical water-content variation in the embankment. The simplest choice for $\alpha_i(\theta)$ is to consider a linear interpolation between the values of water content measured at the N instrumented sections, as shown in Fig. 12(c), so that

$$\alpha_i(\theta) = \begin{cases} 1 & \text{for} \quad \theta = \theta_i & \forall i \in (1,\ldots,N) \\ 0 & \text{for} \quad \theta = \theta_{j\neq i} & \forall i,j \in (1,\ldots,N) \\ 1 - \dfrac{(\theta-\theta_i)}{(\theta_{i+1}-\theta_i)} & \text{for} \quad \theta_i \le \theta \le \theta_{i+1} & \forall i \in (1,\ldots,N) \\ 1 + \dfrac{(\theta-\theta_i)}{(\theta_{i-1}-\theta_i)} & \text{for} \quad \theta_{i-1} \le \theta \le \theta_i & \forall i \in (1,\ldots,N) \end{cases} \tag{3}$$

In general, it is advisable to instrument cross sections forming equal angles between them so that all the weight functions have the same periodicity in θ. Two is suggested as the minimum number of sections required for the procedure to work.

Analogously, with regard to the symmetrical part of the water-content variation, $w^s_k = w^s(x,s,z,t=t_k)$ is obtained as the weighted average of the values of water content, $w^s_{i;k} = w^s(x,s=s_i,z,t=t_k)$, recorded in the N instrumented cross sections at $t=t_k$

$$w^s_k(x,s,z) = w^s(x,s,z,t=t_k) = \sum_{i=1}^{N} w^s_{i;k}(x,z)\cdot\beta_i(s) \tag{4}$$

with $\beta_i(s)$ = weight functions that depend on s rather than on θ. Considering again a linear interpolation between the water content values measured at the N instrumented sections, as shown in Fig. 12(d), $\beta_i(s)$ are here defined as

$$\beta_i(s) = \begin{cases} 1 & \text{for} \quad s = s_i & \forall i \in (1,\ldots,N) \\ 0 & \text{for} \quad s = s_{j\neq i} & \forall i,j \in (1,\ldots,N) \\ 1 - \dfrac{(s-s_i)}{(s_{i+1}-s_i)} & \text{for} \quad s_i \le s \le s_{i+1} & \forall i \in (1,\ldots,N) \\ 1 + \dfrac{(s-s_i)}{(s_{i-1}-s_i)} & \text{for} \quad s_{i-1} \le s \le s_i & \forall i \in (1,\ldots,N) \end{cases} \tag{5}$$

Unlike the case of the α_i functions, for $0 \le s \le s_1$, $\beta_1 = 1$, whereas for $s_N \le s \le L$, $\beta_N = 1$, with L being the total length of the embankment. This means that for $0 \le s \le s_1$, $w^s(x,s,z,t=t_k) = w^s(x,s=s_1,z,t=t_k)$, whereas for $s_N \le s \le L$, $w^s(x,s,z,t=t_k) = w^s(x,s=s_N,z,t=t_k)$. This is because in the regions $0 \le s \le s_1$ and $s_N \le s \le L$, water content measurements are available only for one section, so no interpolation can be carried out. Obviously, when choosing the locations of the 1st and nth cross sections, care should be taken to minimize the length of the longitudinal segments $s_1 - 0$ and $L - s_N$.

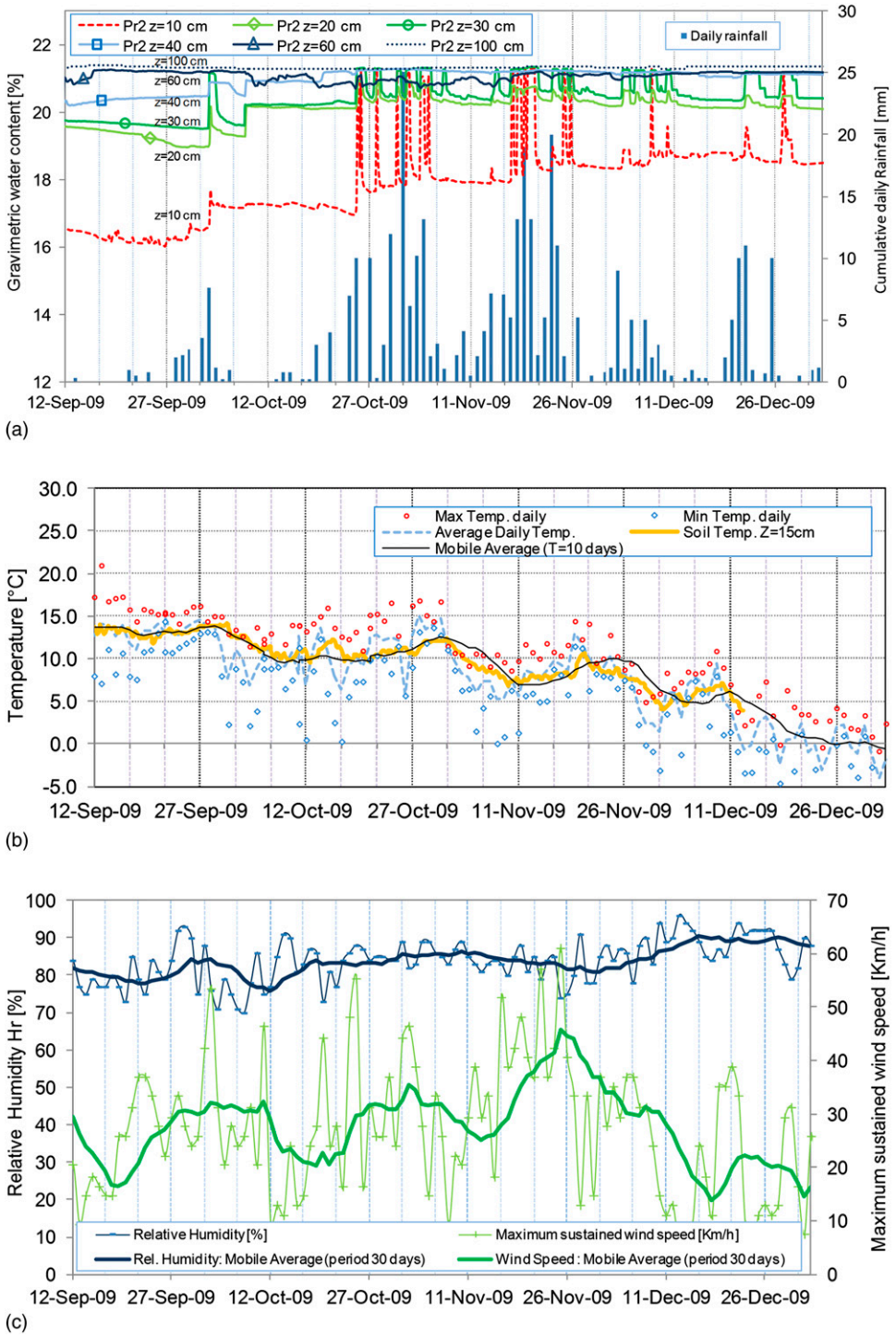

Fig. 9. Winter 2009 (Cross Section B): (a) evolution of gravimetric water content and rainfall record; (b) average of maximum and minimum daily air temperature and ground temperature measured at 10-cm depth; (c) relative humidity and wind speed: thin line follows daily variation, whereas thick line is mobile average over 10 days

The water content at any point of the embankment can now be obtained substituting Eqs. (3) and (5) into Eq. (1)

$$w_k(x,s,z) = w(x,s,z,t=t_k) = \sum_{i=1}^{N} w^a_{i;k}(x,z)\cdot\alpha_i(\theta) + \sum_{i=1}^{N} w^s_{i;k}(x,z)\cdot\beta_i(s) \quad (6)$$

In this case $N=2$, so $w_k(x,s,z)$ is calculated as

$$w_k(x,s,z) = w(x,s,z,t=t_k) = w^a(x,s=s_1,z,t=t_k)\cdot\alpha_1(\theta) + w^a(x,s=s_2,z,t=t_k)\cdot\alpha_2(\theta) + w^s(x,s=s_1,z,t=t_k)\cdot\beta_1(s) + w^s(x,s=s_2,z,t=t_k)\cdot\beta_2(s) \quad (7)$$

where 1 and 2 = Sections A and B, respectively. Note that Eq. (7) provides an analytical expression for the water content at any point

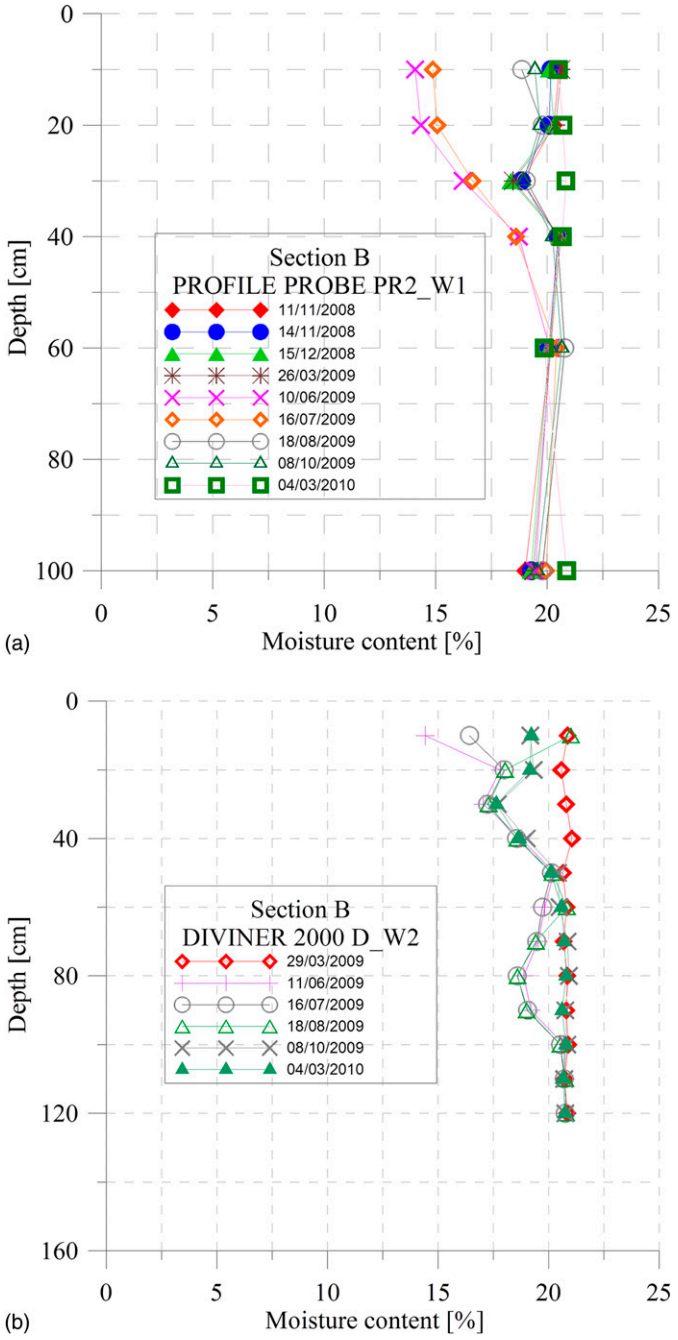

Fig. 10. Examples of profiles of water content at different times in Cross Section B: (a) obtained by PR; (b) obtained by DV

of the embankment at the discrete time points t_k. So, provided that sufficiently small space intervals between instrumented cross sections and sufficiently small time intervals are used, the water content in the embankment could, in principle, be monitored as accurately as desired. So, one may be tempted to conclude that the use of the geotechnical suite alone is good enough for the health monitoring of the embankment. However, the maintenance costs of the geotechnical suite over the typical life span of flood-defense earth embankments (at least 50 years but more often 100–200 years) are higher than the costs for a monitoring program based on geophysical measurements, which only entail noninvasive, periodic walk-over surveys. More importantly, only two sections were used here. With regards to this point, in the authors' opinion, the proposed geotechnical suite may be used as the only monitoring method, but to obtain accurate results, many more sections in the embankment should be monitored. If only a few sections are used to keep the monitoring costs within affordable limits, geophysical probes are necessary to integrate the discrete geotechnical data with spatially continuous measurements acquired along the entire embankment. Such a procedure is subsequently detailed.

Integration of Geophysical Data with Geotechnical Suite

Herein, the variable σ will be used to represent the ground electrical conductivity, which is a function of both space and time; hence, $\sigma = \sigma(x, s, z, t)$. However, electromagnetic probes provide a measure of σ that is averaged over a prismatic volume of ground, where the induced electrical field is nonzero. Considering a generic cross section of the embankment, the authors define

$$\overline{\sigma}(s,t) = \frac{\int_{A_{\mathrm{CMD}}} w(x,s,z,t)\,dx\,dz}{A_{\mathrm{CMD}}} \tag{8}$$

with $A_{\mathrm{CMD}} = b \cdot d$, where b = distance between the two ends of the electromagnetic probe (hence corresponding to the width of the portion of the embankment cross section where the induced electrical field is nonzero) and d = so-called effective depth (i.e., the depth of the induced electromagnetic field). Note that A_{CMD} is independent of the cross section considered. This means that its size does not vary with s, but depends on the type of electromagnetic probe used (for this reason, the authors called it A_{CMD}). The effective depth is a function of the type of ground and of the vertical distance from the portable device to the ground level. The variable d is an unknown that the authors determined by trial and error; they selected the value that provided the best correlation between the electrical conductivity and the water content, as shown later.

In Fig. 13(a), the measurements taken by the CMD-2 device at six time points along the entire embankment, $\overline{\sigma}_k(s) = \overline{\sigma}(s, t = t_k)$, are shown. It emerges that the shapes of the curves are approximately the same for all the times considered. Now, the spatial average of $\overline{\sigma}(s,t)$ over the entire embankment length is introduced as

$$\overline{\overline{\sigma}}(t) = \frac{\int_{s=0}^{s=L} \overline{\sigma}(s,t)\,ds}{L} \tag{9}$$

where the second above-score bar = spatial average over the longitudinal coordinate s. Then, the normalized cross-sectional average electrical conductivity can be introduced as

$$\overline{\sigma}_0(s,t) = \frac{\overline{\sigma}(s,t)}{\overline{\overline{\sigma}}(t)} \tag{10}$$

The normalized measurements taken at times t_k [i.e., $\overline{\sigma}_{0_k} = \overline{\sigma}_0(s, t = t_k)$] are plotted in Fig. 13(b). From the figure, it emerges that the curves coincide almost perfectly. This leads to the conclusion that the average of $\overline{\sigma}_{0_k} = \overline{\sigma}_0(s, t = t_k)$ over time

$$\underline{\overline{\sigma}}_0(s) = \underset{k}{\text{average}}\,\overline{\sigma}_0(s, t = t_k) = \underset{k}{\text{average}}\left[\frac{\overline{\sigma}(s, t = t_k)}{\overline{\overline{\sigma}}(t = t_k)}\right] \tag{11}$$

can be considered as the representative curve of the conductivity of the embankment. Note that herein the underscore bar denotes time averaging. The measurements were taken by an operator walking above the center of the embankment's horizontal upper surface. Therefore, they

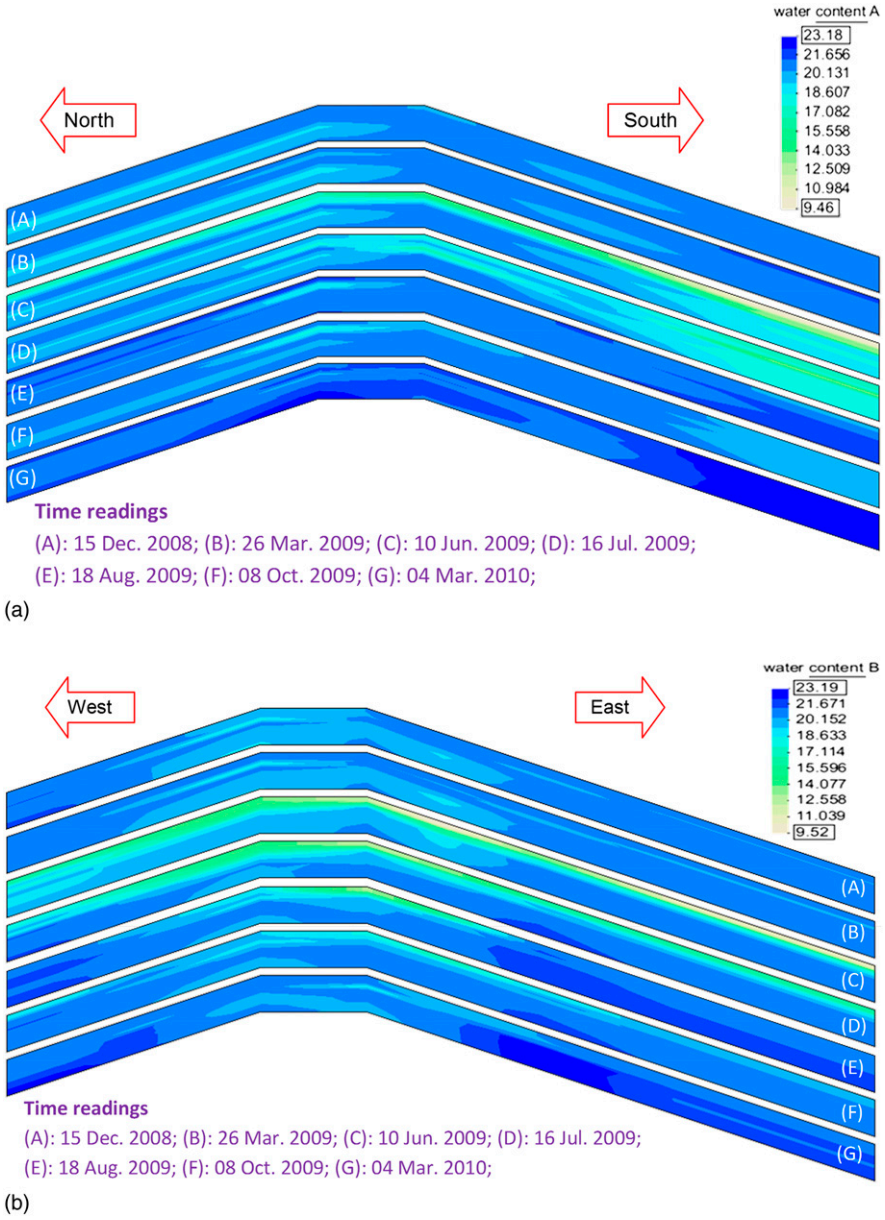

Fig. 11. Contours of water content at different times over period of 1.5 years: (a) in Cross Section A; (b) in Cross Section B

cannot detect any conductivity variation due to different cross-sectional orientations (i.e., they are independent of the angle θ). The time-independent function $\underline{\overline{\sigma}}_0(s)$ can be thought of as a unique identifier of the embankment expressing the variation of the conductivity along the s-coordinate due to the variation of the geometrical, hydraulic, and lithological properties of cross sections and the effects of the exposure to weather conditions independent of cross-sectional orientation (i.e., cross-sectionally symmetric). On the other hand, the function $\overline{\overline{\sigma}}(t)$ reflects the temporal effect of climatic variations (e.g., rainfall, wind, or temperature variations) and aging on the ground conductivity.

Now, the ground conductivity function, $\overline{\sigma}(s,t)$, can be split into the product of the time-independent dimensionless function $\underline{\overline{\sigma}}_0(s)$ and the space-independent dimensional function $\overline{\overline{\sigma}}(t)$

$$\overline{\sigma}(s,t) = \underline{\overline{\sigma}}_0(s) \cdot \overline{\overline{\sigma}}(t) \tag{12}$$

In the following, it will be shown that this split is a necessary step to find a correlation between the water content and the electrical conductivity. First, the authors define the average water content in the portion of the embankment cross sections where the electromagnetic field is nonzero (i.e., A_{CMD})

$$\overline{w}(s,t) = \frac{\int_{A_{\mathrm{CMD}}} w(x,s,z,t)\,dxdz}{A_{\mathrm{CMD}}} \tag{13}$$

Analogously to $\overline{\sigma}(s,t)$, $\overline{w}(s,t)$ can be split into two functions: a time-independent dimensionless function, $\underline{\overline{w}}_0(s)$, which accounts for the effect of cross-sectional orientation and position on the groundwater content, and the space-independent dimensional function, $\overline{\overline{w}}(t)$, which accounts for the effect of climatic variations and aging on the groundwater content

$$\overline{w}(s,t) = \underline{\overline{w}}_0(s) \cdot \overline{\overline{w}}(t) \tag{14}$$

where $\overline{\overline{w}}(t)$ = spatial average of the water content of the cross-sectional area A_{CMD} and along the longitudinal coordinate s

$$\overline{\overline{w}}(t) = \frac{\int_0^L \frac{\int_{A_{CMD}} \left[\sum_{i=1}^{N} w^a(x, s = s_i, z, t) \cdot \alpha_i(\theta) + \sum_{i=1}^{N} w^s(x, s = s_i, z, t) \cdot \beta_i(s)\right] dxdz}{A_{CMD}} ds}{L} \tag{15}$$

To look for a correlation between the measured electrical conductivity and water content, the time dependent functions $\overline{\overline{w}}(t)$ and $\overline{\overline{\sigma}}(t)$ will be considered. Before doing so, the strong dependency exhibited by the ground electrical conductivity on the temperature must be accounted for (Keller and Frischknecht 1966). Recently, Hayley et al. (2007) investigated this dependency for a range of temperatures similar to the range exhibited in the monitored embankment (with the temperature varying between 0 and 25°C) on a glacial till, finding a linear dependency of the type

$$\sigma = \sigma_{25}[C(T - 25) + 1] \tag{16}$$

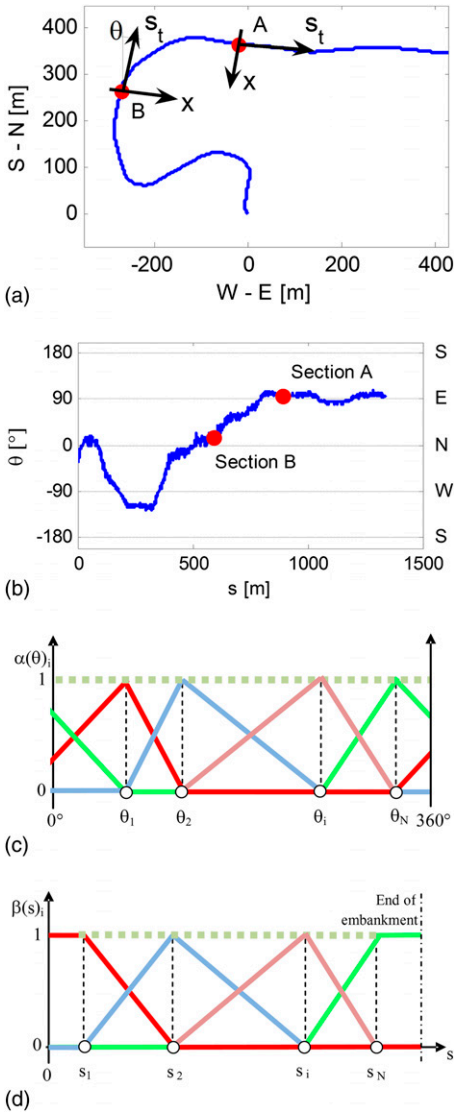

Fig. 12. (a) Plan view of embankment layout; (b) orientation of longitudinal axis of embankment with respect to north; (c) α weight functions against cross-sectional orientation; (d) β weight functions against longitudinal coordinate s

with σ = electrical conductivity measured at the temperature T; and constant $C = 0.02$. To account for the effect of the temperature on the measured electrical conductivity, the authors expressed all of the measured values relative to the same reference temperature before correlating them to the water content. As shown in Hayley et al. (2007), manipulating Eq. (16), the following expression for the calculation of σ relative to the chosen reference temperature is obtained

$$\sigma_{ref} = \sigma \frac{1 + C(T_{ref} - 25)}{1 + C(T - 25)} \tag{17}$$

with σ_{ref} = value of electrical conductivity relative to the reference temperature, T_{ref}. Here, the authors chose $T_{ref} = 15$°C to minimize the amount of temperature compensation. Using Eq. (17), the authors calculated σ_{ref} from the in situ values of σ and T.

In Fig. 14, the water content measured at the time points t_k, $\overline{\overline{w}}(t = t_k)$, is plotted against the electrical conductivity measured at the same time points, $\overline{\overline{\sigma}}_{ref}(t = t_k)$. It emerges that the relationship between $\overline{\overline{w}}(t)$ and $\overline{\overline{\sigma}}_{ref}(t)$ is well captured by a linear function so that

$$\overline{\overline{w}}(t) = m\overline{\overline{\sigma}}_{ref}(t) + q \tag{18}$$

with m and q determined by best fit (Fig. 14). Substituting Eq. (17) into Eq. (18), it becomes

$$\overline{\overline{w}}(t) = m\overline{\overline{\sigma}}(t) \frac{1 + C(T_{ref} - 25)}{1 + C(T - 25)} + q \tag{19}$$

Eq. (19) links the in situ measured water content to the in situ measured electrical conductivity.

To work out the water content at any point of the embankment, $w(x, s, z, t)$, the space-independent dimensional function, $\overline{\overline{w}}(t)$, must be multiplied by a normalized time-independent function, $\underline{w}_0(x, s, z)$, so that

$$w(x, s, z, t) = \underline{w}_0(x, s, z) \cdot \overline{\overline{w}}(t) \tag{20}$$

Following the approach adopted in the "Derivation of Water Content Function from Data Retrieved by Geotechnical Suite" section, $w_0(x, s, z)$ is split into the summation of two parts, an antisymmetrical part and a symmetrical part

$$\underline{w}_0(x, s, z) = \underline{w}_0^a(x, s, z) + \underline{w}_0^s(x, s, z) \tag{21}$$

As in the "Derivation of Water Content Function from Data Retrieved by Geotechnical Suite" section, the authors assume $\underline{w}_0^a(x, s, z)$ to be the time average of the linear combination of the functions expressing the normalized water content measured at times t_k at the N instrumented cross sections, $w_{0_{i,k}}^a(x, z)$

$$\underline{w}_0^a(x, s, z) = \underset{k}{\text{average}} \left[\sum_{i=1}^{N} w_{0_{i,k}}^a(x, z) \cdot \alpha_i(\theta) \right] \tag{22}$$

According to standard normalization procedures, $w_{0_{i,k}}^a(x, z)$ and $w_{0_{i,k}}^s(x, z)$ are defined as

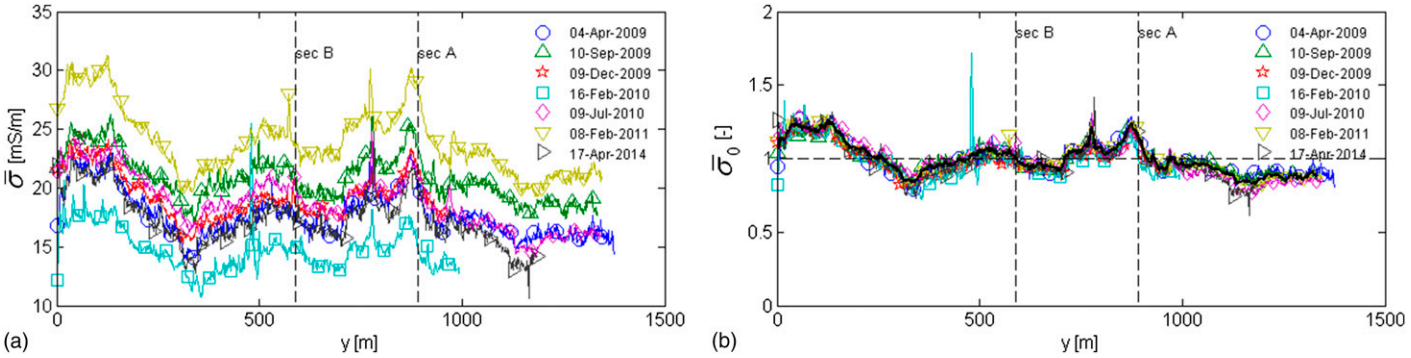

Fig. 13. (a) Electrical conductivity measurements along embankment at seven different times; (b) normalized values of conductivity measurements

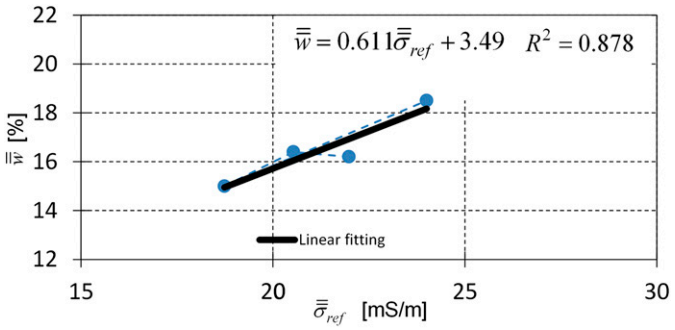

Fig. 14. Correlation obtained over monitored 2-year time period between $\overline{\overline{\sigma}}_{\text{ref}}$, electrical conductivity at chosen reference temperature ($T_{\text{ref}} = 15°\text{C}$), and $\overline{\overline{w}}$ calculated for effective depth of $d = 0.2$ m

$$w^a_{0_{i;k}}(x,z) = w^a_0(x, s = s_i, z, t = t_k) = \frac{w^a(x, s = s_i, z, t = t_k)}{\frac{\int_{A_i} w^a(x, s = s_i, z, t = t_k)dxdz}{A_i}}$$

$$w^s_{0_{i;k}}(x,z) = w^s_0(x, s = s_i, z, t = t_k) = \frac{w^s(x, s = s_i, z, t = t_k)}{\frac{\int_{A_i} w^s(x, s = s_i, z, t = t_k)dxdz}{A_i}} \tag{23}$$

with A_i = area of the ith cross section.

For the symmetrical function $\underline{w}^s_0(x,s,z)$, the authors assume the following expression:

$$\underline{w}^s_0(x,s,z) = \overline{w}^s(s,t)\cdot\underline{\overline{\sigma}}_0(s) = \underset{k}{\text{average}}\left[\sum_{i=1}^{N} w^s_{0_{i;k}}(x,z)\cdot\beta_i(s)\right]\underline{\overline{\sigma}}_0(s) \tag{24}$$

The dimensionless function $\underline{\overline{\sigma}}_0(s)$ accounts for the spatial variation of the water content along the longitudinal direction of the embankment detected by the geophysical probe during walk-over surveys. Eq. (24) constitutes an important improvement in comparison with Eq. (4), because the time average of the linear combination of the water content values measured at the N instrumented cross sections, $\underset{k}{\text{average}}\,[\sum_{i=1}^{N} w^s_{0_{i;k}}(x,z)\cdot\beta_i(s)]$, is adjusted by multiplication with $\underline{\overline{\sigma}}_0(s)$ to account for the spatial variation of the conductivity detected by the geophysical survey along the longitudinal direction. The advantage of using geophysics is now apparent, because geophysics provides measurements that are continuous along the spatial coordinate s. This allows the improvement of the quality of the estimated water content, especially in the zones of the embankment farthest away from the geotechnically instrumented cross sections.

So far, the symmetrical component of the water content, $\underline{w}^s_0(x,s,z)$, has been related to the geophysical measurements of the variation of the ground electrical conductivity along the s-coordinate (i.e., dependent on the cross-sectional position). In principle, it should also be possible to relate the antisymmetrical component of the water content, $\underline{w}^a_0(x,s,z)$, to the geophysical measurements of the variation of the ground electrical conductivity due to cross-sectional orientation (i.e., dependent on the angle θ). Recall that the geophysical measurements were taken by an operator walking above the center of the embankment's horizontal upper surface, where the effect of cross-sectional orientation is negligible, so the measurements are a function of the cross-sectional position only (hence, they are a function of the s-coordinate only). To correlate the electrical conductivity to the antisymmetrical part of the water content, measurements of the electrical conductivity along more than one path would be needed, with some of them being along the embankment flanks. However, these measurements would be likely affected by a large error, because it is very difficult to walk for long distances on the embankment flanks (which are variously inclined) while keeping a constant geometrical height (z-coordinate).

Now, substituting Eqs. (19), (22), and (24) into Eq. (20), the water content at the time t_l of the geophysical measurement, $w(x,s,z,t=t_l)$, can be derived as a function of the average cross-sectional ground conductivity, $\overline{\sigma}(s,t=t_l)$

$$w(x,s,z,t=t_l) = \left\{ \underset{k}{\text{average}}\left[\sum_{i=1}^{N} w^a_0(x,s=s_i,z,t=t_k)\cdot\alpha_i(\theta)\right] + \underset{k}{\text{average}}\left[\sum_{i=1}^{N} w^s_0(x,s=s_i,z,t=t_k)\cdot\beta_i(s)\right] \cdot\underline{\overline{\sigma}}_0(s)\right\}\cdot\left[m\frac{\overline{\sigma}(s,t=t_l)}{\underline{\overline{\sigma}}_0(s)}\frac{1+C(T_{\text{ref}}-25)}{1+C(T-25)}+q\right] \tag{25}$$

Eq. (25) provides the analytical expression to be used to monitor the water content in the embankment carrying out periodic walk-over surveys over a time period that can be much longer than the time of the activity of the geotechnical suite (i.e., $t_l \gg t_k$).

Plotted in Fig. 15 are the spatial distributions of the water content calculated using Eq. (25) in four cross sections ($s = 2, 182, 672$, and

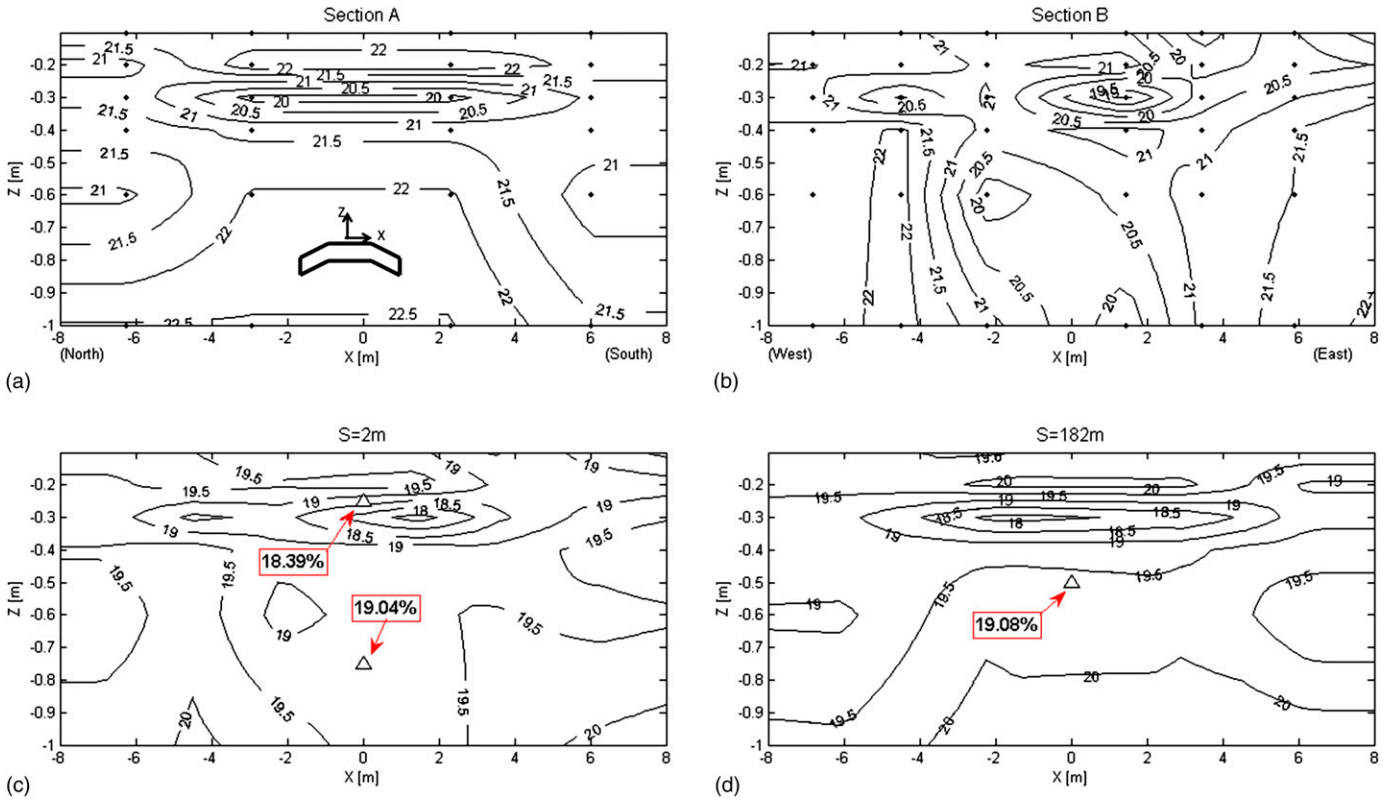

Fig. 15. Values of water content estimated from electrical conductivity measured by CMD-2 during walk-over survey carried out on April 17, 2014, using proposed methodology: (a) water content in Section A; (b) water content in Section B; (c) water content at $s = 2$ m; (d) water content at $s = 182$ m; triangles in Figs. 15(c and d) indicate value of water content measured in laboratory from retrieved in situ samples

972 m) from the electrical conductivity profile of the embankment, which were measured during a walk-over survey carried out on April 17, 2014 (so, for $t_l > t_k$). To provide a validation of the proposed method, a few soil samples were retrieved from the embankment and brought to the laboratory for accurate measurement. In the plots of Figs. 15(c and d), the experimental values of the water content are reported as triangles. Comparing the predictions of the method with the experimental measurements of the water content, the predictions are in very good agreement with the experimentally measured values. This is quite remarkable, especially in light of the fact that the measurements were taken at a time (April 17, 2014) well beyond the 2-year period within which the geotechnical and geophysical measurements had been performed to calibrate the model.

Options for Long-Term Monitoring

In light of the results, three options of increasing accuracy and cost emerge for the monitoring of the embankment water content over time. The first and cheapest option consists of using meteorological data only, the second and more expensive option relies on periodic walk-over surveys to retrieve geophysical data using electromagnetic probes, and the third and most expensive option requires both periodic walk-over surveys to retrieve geophysical data and measurements in a number of cross sections from a permanent geotechnical suite. The first option requires the use of the geotechnical suite for an initial, limited period of time without any periodic (geotechnical or geophysical) measurements at subsequent times. For the second option, the integration of the geotechnical data with the geophysical data ("Integration of Geophysical Data with Geotechnical Suite" section) is carried out for a limited initial period only, whereas for the third option, the integration is carried out repeatedly during the whole lifetime of the structure. The second option provides predictions that are more robust than those of the first one, because the first option relies on a relationship between the meteorological data and the variation of the water content established over the initial time of monitoring, which is expected to change over time with the aging of the structure. Depending on the importance of the structure and the available financial resources, the authorities in charge of the maintenance of the embankments can select the most suitable option.

Proposal for Susceptibility Index to Desiccation Fissuring

Here, a proposal is put forward for a susceptibility index for a failure mechanism that can be directly related to the presence of desiccation cracks. Cooling and Marsland (1954), Marsland and Cooling (1958), and, more recently, Morris et al. (2007) and Dyer et al. (2009) have described failure mechanisms that take place when water overflows the embankment crest in the presence of an interconnected pattern of vertical and horizontal cracks underneath the horizontal upper surface and the landward flank of the embankment. Overtopping water seeping downward into the open cracks leads to the progressive uplift and removal of intact blocks of ground, first from the landward flank and subsequently from the horizontal upper surface [Fig. 16(a)]. This failure mechanism is particularly dangerous, because it leads to the development of a fast breach, which can lead to quick flooding. The formation of extensive cracks is also detrimental for the structure, because it favors internal piping.

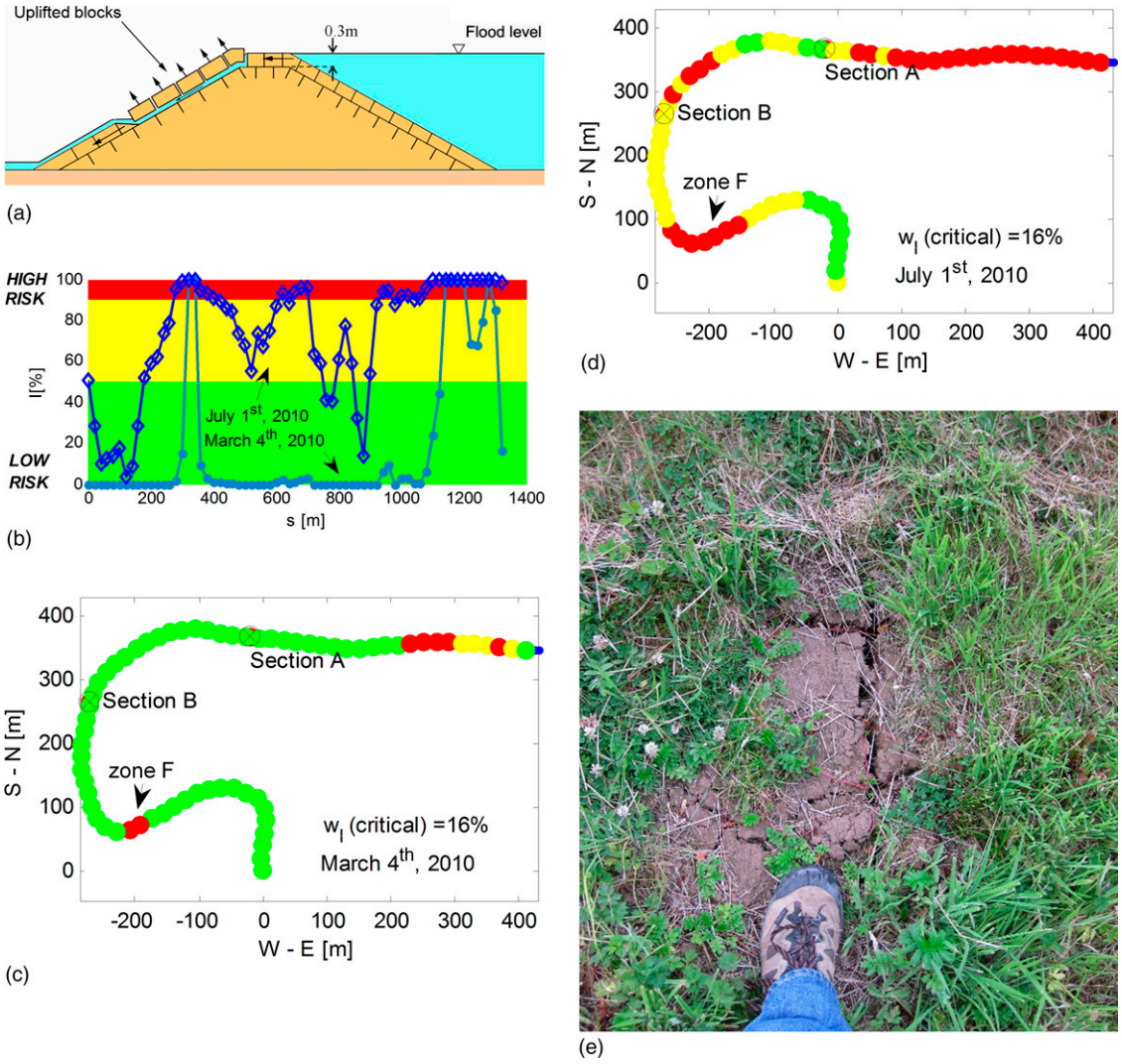

Fig. 16. (a) Representation of total area A_Ω considered in calculation of susceptibility index (figure modified from Dyer et al. 2009); (b) calculated susceptibility indexes along embankment for March 4, 2010, and July 1, 2010; (c) risk map of embankment drawn on March 4, 2010; (d) risk map of embankment drawn on July 1, 2010; (e) surficial crack system taken in Zone F of Figs. 16(c and d)

Tests run by Tang et al. (2011) on clay samples of various shapes show that after four wetting-drying cycles, the onset of cracks can be uniquely related to the value of the soil water content (i.e., it becomes independent of the wetting-drying history). In Costa et al. (2013), it is shown that once the water content in clayey soils goes below a threshold value near the plastic limit, w_{plastic}, no additional cracks are formed. The determination of a threshold value of the water content at which an interconnected network of cracks is formed and, equally, the determination of a critical threshold value for piping failure are challenging issues that are outside the scope of this paper. Unsaturated soil mechanics and the formation of desiccation fissures in cohesive soils are topics of intense current research. Therefore, it is plausible to expect that in the future, with further results becoming available, it will be possible to establish a better susceptibility index based on less-crude assumptions. The index proposed here was conceived to provide a purely qualitative indication about which zones of the embankment are liable to fissuring, so it should not be relied upon for quantitative predictions regarding the level of hazard or the likelihood of failure in these zones. Here, for the sake of simplicity, the authors assumed this threshold to coincide with the plastic limit (w_{plastic}) of the till. As a first approximation, the authors also assumed that the ground zones where the water content is below the plastic limit are fissured so that the portion of the cross section where $w < w_{\text{plastic}}$ is considered fully fissured, whereas the portion where $w > w_{\text{plastic}}$ is considered intact. The sought susceptibility index has to reflect how far a cross section is from the critical condition leading to failure. Hence, the index proposed here is defined as the ratio of the sectional area where cracks have formed, A_{fis}, over the sectional area required for the development of the considered failure mechanism, A_Ω

$$I = \frac{A_{fis}}{A_\Omega} \quad \text{with} \quad 0 < I < 1 \tag{26}$$

The size of A_Ω is a property of the ground. In Dyer et al. (2009), a maximum characteristic depth for the formation of an interconnected network of cracks 0.6 m deep was observed in trial pits excavated in embankments made of glacial tills similar to the embankment investigated in this paper. Therefore, a depth of 0.6 m

was used to determine the sectional domain used for the calculation of A_Ω [Fig. 16(a)].

In Fig. 16(b), the function $I(s)$ representing the value of the index along the embankment was plotted for two different time points. It can be observed that in the winter the susceptibility index is nil (i.e., no fissuring is expected) in most of the embankment, apart from two rather small zones where the index spikes up to 1. Conversely, in the summer the index assumes values larger than 0 in the whole embankment. Fig. 16(b) is sufficient to identify the zones of the embankment that are most in need of remedial measures. However, it may be useful to define the categories of risk for intervention protocols whereby the type and urgency of the intervention are related to the established categories. Here, as an example, three categories were established: no risk, associated with $0 < I < 0.5$; moderate risk, associated with $0.5 < I < 0.90$; and high risk, associated with $0.90 < I < 1$. In the zones classed as high risk ($I > 0.9$), cracks were observed during both the winter and the summer periods [Fig. 16(e)]. Also, the plots in Figs. 16(c and d) provide user-friendly visualizations of the locations of the most critical zones in the embankment.

Conclusions

In this paper, a cost-effective methodology for the quantitative assessment of the potential for desiccation fissuring for earthen embankments and tailing dams was established. Currently, the monitoring and condition assessment of embankments is performed by visual inspections at set intervals. The proposed methodology is simple and suitable for use over the entire lifetime of the structures by the authorities in charge of their maintenance. This methodology paves the way for a radical improvement over the methods currently used by moving to a quantitative assessment of the liability of long embankments (levees) to desiccation fissuring.

The methodology is based on the use of a suite of standard geotechnical probes for the measurement of the water content in a limited number of locations in the embankment integrated with periodic, noninvasive geophysical measurements from walk-over surveys using portable electromagnetic probes. Most of the data from the geotechnical suite were acquired by automatic reading systems involving minimal labor. An innovative calibration procedure was used to calibrate the geotechnical probes (THP, PR, DV, etc.) in situ by cross-comparison.

An index of the susceptibility to desiccation-induced deterioration was defined. Contour plots of the calculated index provide an easy-to-use visual tool to monitor the health state of the structure and identify the most critical zones to prioritize remedial interventions. Also, a protocol to monitor the susceptibility of earthen embankments to desiccation-induced deterioration over their lifespans is proposed based on three hierarchical levels of increasing cost and accuracy. The first and cheapest option consists of using meteorological data only, the second and more expensive option relies on periodic walk-over surveys to retrieve geophysical data from the site, and the third and most expensive option requires both periodic walk-over surveys to retrieve geophysical data and measurements in a number of cross sections from a permanent geotechnical suite.

Acknowledgments

This research was carried out within the project "Long Term Deterioration of Flood Embankments" funded by the Scottish Executive and by Grant 0708 from the Institution of Civil Engineers (ICE) Research and Development Enabling Fund. Mr. Marco Secondi is thanked for his help in setting out the instrumentation and acquiring and managing the database from the field. Ms. Chiara Grisanti is thanked for contributing to Figs. 9, 10, and 15.

Notation

The following symbols are used in this paper:

A_{CMD} = portion of cross-sectional area where induced electric field is nonzero;

A_{fis} = portion of cross-sectional area where $w < w_{\mathrm{plastic}}$;

A_i = area of cross section i;

A_Ω = portion of cross-sectional area with interconnected cracks causing decrease of bearing capacity;

C = constant;

I = susceptibility index;

i = integer indicating number of embankment cross section considered;

k = integer indicating chronological sequence of measurement performed;

m = slope coefficient for linear interpolation in Fig. 14;

P = vertical line (point on embankment surface) in Cross Section B of embankment;

q = intercept coefficient for linear interpolation in Fig. 14;

s = global curvilinear coordinate along longitudinal axis of embankment;

s_t = local Cartesian coordinate orthogonal to x and z;

$\overline{w}(s,t)$ = cross-sectional water content average; water content is averaged over portion of embankment cross section where induced electric field is nonzero (A_{CMD});

$\overline{\overline{w}}(t)$ = space average of water content (average over entire embankment); water content is averaged over portion of embankment cross section where induced electric field is nonzero (A_{CMD});

$w(x,s,z,t)$ = water content;

$w^a(x,s,z,t)$ = antisymmetrical part of cross-sectional water content;

$w_{i;k} = w(x, s = s_i, z, t = t_k)$ = water content measured in cross section i at time t_k;

$w_k = w(x,s,z,t = t_k)$ = water content measured at time t_k;

$w_P = w(x = x_P, s = s_P, z, t)$ = water content measured along vertical line P;

w_{plastic} = water content at plastic limit;

$w^s(x,s,z,t)$ = symmetrical part of cross-sectional water content;

$\underline{\overline{w}}_0(s)$ = time average of normalized cross-sectional average water content;

$\overline{w}_0(s,t)$ = normalized cross-sectional average water content;

X = global Cartesian coordinate;
x = local Cartesian horizontal coordinate in embankment cross section;
Y = global Cartesian coordinate;
Z = global Cartesian coordinate;
z = local vertical downward Cartesian coordinate;
α = weight function;
β = weight function;
θ = angle of s_t with X-axis; it indicates orientation of cross section with regard to global Cartesian coordinate system;
σ = electrical conductivity;
$\overline{\sigma}(s,t)$ = cross-sectional average electrical conductivity; electrical conductivity is averaged over portion of embankment cross section where induced electric field is nonzero (A_{CMD});
$\overline{\overline{\sigma}}(t)$ = space average of electrical conductivity (average over entire embankment); electrical conductivity is averaged over portion of embankment cross section where induced electric field is nonzero (A_{CMD});
$\overline{\sigma}_k(s) = \overline{\sigma}(s, t = t_k)$ = cross-sectional electrical conductivity average measured at time t_k;
$\underline{\overline{\sigma}}_0(s)$ = time average of normalized cross-sectional average electrical conductivity; and
$\overline{\sigma}_0(s,t)$ = normalized cross-sectional average electrical conductivity.

References

Allsop, W., et al. (2007). "Failure mechanisms for flood defence structures." *Research Rep. T04-06-01*, FLOODsite Consortium, HR Wallingford, Oxfordshire, U.K.

Andersen, G. R., Chouinard, L. E., Bouvier, C., and Back, W. E. (1999). "Ranking procedure on maintenance tasks for monitoring of embankment dams." *J. Geotech. Geoenviron. Eng.*, 10.1061/(ASCE)1090-0241(1999)125:4(247), 247–259.

ASCE/EWRI Task Committee on Dam/Levee Breaching. (2011). "Earthen embankment breaching." *J. Hydraul. Eng.*, 10.1061/(ASCE)HY.1943-7900.0000498, 1549–1564.

ASTM. (2013). "Standard specification for woven wire test sieve cloth and test sieves." *E11*, West Conshohocken, PA.

Aubeny, C. P., and Lytton, R. L. (2004). "Shallow slides in compacted high plasticity clay slopes." *J. Geotech. Geoenviron. Eng.*, 10.1061/(ASCE)1090-0241(2004)130:7(717), 717–727.

Charles, J. A. (2008). "The engineering behaviour of fill materials: The use, misuse and disuse of case histories." *Géotechnique*, 58(7), 541–570.

Cooling, L. F., and Marsland, A. (1954). "Soil mechanics studies of failures in the sea defence banks of Essex and Kent." *Proc., Conf. on the North Sea Floods of 31 January/1 February, 1953: A Collection of Papers Presented at the Institution in December 1953*, Institution of Civil Engineers (ICE), London, 58–73.

Costa, S., Kodikara, J., and Shannon, B. (2013). "Salient factors controlling desiccation cracking of clay in laboratory experiments." *Géotechnique*, 63(1), 18–29.

D'Elisio, C. (2007). "Breaching of sea dikes initiated by wave overtopping: A tiered and modular modeling approach." Ph.D. thesis, Univ. of Braunschweig, Braunschweig, Germany, and Univ. of Florence, Florence, Italy.

De Vita, P., Di Maio, R., and Piegari, E. (2012). "A study of the correlation between electrical resistivity and matric suction for unsaturated ash-fall pyroclastic soils in the Campania region (southern Italy)." *Environ. Earth Sci.*, 67(3), 787–798.

Di Maio, R., and Piegari, E. (2011). "Water storage mapping of pyroclastic covers through electrical resistivity measurements." *J. Appl. Geophys.*, 75(2), 196–202.

Dyer, M., Utili, S., and Zielinski, M. (2009). "Field survey of desiccation fissuring of flood embankments." *Proc. Inst. Civ. Eng. Water Manage.*, 162(3), 221–232.

Environment Agency. (2006). "Condition assessment manual." *Rep. DR 166_03_SD01*, Bristol, U.K.

GF Instruments. (2011). "Short guide for electromagnetic conductivity survey." ⟨http://www.gfinstruments.cz/version_cz/downloads/CMD_Short_guide-2013.pdf⟩ (Apr. 15, 2014).

GiD [Computer software]. Barcelona, Spain, International Center for Numerical Methods in Engineering.

Hayley, K., Bentley, L. R., Gharibi, M., and Nightingale, M. (2007). "Low temperature dependence of electrical resistivity: Implications for near surface geophysical monitoring." *Geophys. Res. Lett.*, 34(18), L18402.

Highways Agency. (2006). *Manual of contract documents for highway works: Specification for highway works*, Vol. 1, Birmingham, U.K. ⟨http://www.dft.gov.uk/ha/standards/mchw/vol1/pdfs/series_0600.pdf⟩ (Apr. 9, 2014).

International Center for Numerical Methods in Engineering. (2014). "GiD reference manual." ⟨http://www.gidhome.com/whats-gid⟩ (Feb. 21, 2013).

Keller, G. V., and Frischknecht, F. C. (1966). *Electrical methods in geophysical prospecting*, Pergamon Press, Oxford, U.K.

Konrad, J.-M., and Ayad, R. (1997). "Desiccation of a sensitive clay: Field experimental observations." *Can. Geotech. J.*, 34(6), 929–942.

Marsland, A., and Cooling, L. F. (1958). "Tests on full scale clay flood bank to study seepage and the effects of overtopping." *Internal Rep. No. C562*, Building Research Station, Watford, U.K.

Milly, P., Wetherald, R., Dunne, K., and Delworth, T. (2002). "Increasing risk of great floods in a changing climate." *Nature*, 415(6871), 514–517.

Morris, M., Dyer, M., Smith, P., Falkingham, J., and Simms, J. (2007). "Management of flood defences." *R&D Rep. FD2411*, Defra/Environment Agency (EA), London.

Muñoz-Castelblanco, J. A., Pereira, J. M., Delage, P., and Cui, Y. J. (2012a). "The influence of changes in water content on the electrical resistivity of a natural unsaturated loess." *Geotech. Test. J.*, 35(1), 11–17.

Muñoz-Castelblanco, J. A., Pereira, J. M., Delage, P., and Cui, Y. J. (2012b). "The water retention properties of a natural unsaturated loess from northern France." *Géotechnique*, 62(2), 95–106.

Perry, J., Pedley, M., and Reid, M. (2001). "Infrastructure embankment: Condition appraisal and remedial treatment." *CIRIA Rep. C550*, Construction Industry Research and Information Association (CIRIA), London.

Rodriguez, R., Sanchez, M., Ledesma, A., and Lloret, A. (2007). "Experimental and numerical analysis of desiccation of a mining waste." *Can. Geotech. J.*, 44(6), 644–658.

Shin, H., and Santamarina, J. C. (2011). "Desiccation cracks in saturated fine-grained soils: Particle level phenomena and effective stress analysis." *Géotechnique*, 61(11), 961–972.

Smethurst, J. A., Clarke, D., and Powrie, W. (2012). "Factors controlling the seasonal variation in soil water content and pore water pressures within a lightly vegetated clay slope." *Géotechnique*, 62(5), 429–446.

Tang, C.-S., Cui, Y.-J., Shi, B., Tang, A.-M., and Liu, C. (2011). "Desiccation and cracking behaviour of clay layer from slurry state under wetting–drying cycles." *Geoderma*, 166(1), 111–118.

Utili, S. (2013). "Investigation by limit analysis on the stability of slopes with cracks." *Géotechnique*, 63(2), 140–154.

Wan, C. F., and Fell, R. (2004). "Investigation of rate erosion of soils in embankment dams." *J. Geotech. Geoenviron. Eng.*, 10.1061/(ASCE)1090-0241(2004)130:4(373), 373–380.

Xu, C.-Y., and Singh, V. P. (2001). "Evaluation and generalization of temperature-based methods for calculating evaporation." *Hydrol. Processes*, 15(2), 305–319.

Zhang, Z., Tao, M., and Morvant, M. (2005). "Cohesive slope surface failure and evaluation." *J. Geotech. Geoenviron. Eng.*, 10.1061/(ASCE)1090-0241(2005)131:7(898), 898–906.

Zielinski, M. (2009). "Influence of desiccation fissuring on the stability of flood embankments." Ph.D. thesis, Univ. of Strathclyde, Glasgow, U.K.

Zielinski, M., Sanchez, M., Romero, E., and Sentenac, P. (2011). "Assessment of water retention behaviour in compacted fills." *Proc. Inst. Civ. Eng. Geotech. Eng.*, 164(2), 139–148.